Available online at www.sciencedirect.com

ScienceDirect

Mendeleev Commun., 2024, **34**, 899–901

Mendeleev Communications

Nickel nanoparticles formation during Ni catalyst activation revealed by identical location electron microscopy

Anton E. Dzhusupov[a,b] and Evgeniy O. Pentsak*[a]

[a] *N. D. Zelinsky Institute of Organic Chemistry, Russian Academy of Sciences, 119991 Moscow, Russian Federation. E-mail: p_eugene@ioc.ac.ru*

[b] *Department of Carbon Materials and Natural Energy, D. I. Mendeleev University of Chemical Technology of Russia, 125047 Moscow, Russian Federation*

DOI: 10.1016/j.mencom.2024.10.041

Formation of metallic nickel nanoparticles was observed during nickel catalyst activation in hydrogen flow at high temperature. The scale of change in catalyst morphology was determined *via* identical location electron microscopy.

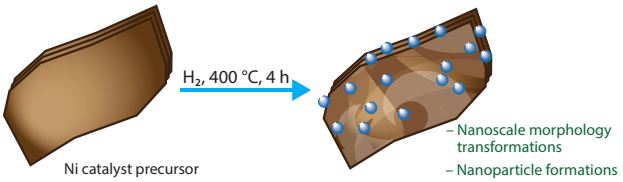

Keywords: nickel, heterogeneous catalysis, hydrogenation, morphology, nanoparticles, electron microscopy, selected area microscopy, identical location electron microscopy (IL EM).

Nickel catalysts have found applications in the most important branches of chemistry, including synthesis of many significant products for basic organic synthesis.[1–10] High loaded Ni catalysts containing up to 95% Ni are important for the production of hydrogen by catalytic pyrolysis of methane, dehydrogenation, hydrogenation, hydrodeoxygenation and various pyrolysis processes.[11–20]

For the preparation of high loaded nickel catalysts and methane conversion, the heterophase sol–gel technique has a number of advantages.[21–25] Features of sol–gel methods are: simplicity of execution, ability to provide a higher content of active metal on the support, high dispersion of the active phase in the catalyst, high efficiency in pyrolysis processes and obtaining the high-quality carbon nanofibers as a by-product.[9,26–29] In these approaches, after synthesis nickel is present on the matrix as an oxide, and silicon forms a net of silicate structures and free silicon oxide, thus preventing the sintering of metal particles.[23]

For catalyst activation, nickel is reduced from Ni^{2+} form to metal (Ni^0).[5] It is believed that catalyst activation is due to reduction to nickel metal. This typically occurs in a hydrogen stream at high temperatures, *e.g.*, in the production of hydrogenation catalysts.[6,20] The temperature-programmed reduction method has been used to determine the optimal reduction temperature.[16,25,30] However, changes in the particle size distribution and morphology during reduction are not enough understood.

The study of the catalytic systems dynamics has a great fundamental interest. It is well known that catalytic systems have been previously considered static, but later the theory has been developed that the dynamic nature of the systems and evolution of the catalytic structure during the chemical reaction affects the catalytic activity.[31]

The basic method of studying the morphology is scanning electron microscopy (SEM). Typically, electron microscopy is used to obtain average parameters based on random particles of a catalyst sample. In this case, different selected catalyst particles are used in the reaction and are being investigated. In contrast, monitoring the same region before and after the reaction allows to determine changes in parameters of the same particles within the same region. For example, small changes in the shape of particles, their relative position or the size of individual particles without a noticeable variation of the average parameters are difficult to observe by measuring the mean size of catalyst particles. In recent years, the development of electron microscopy methods has made possible to obtain important information about dynamic processes in heterogeneous catalytic systems *via* the selected-area microscopy or identical location electron microscopy (IL EM).[32–35] In this work evolution of the nickel catalyst morphology during its activation by hydrogen has been studied in details at three levels of organization of the catalytic system. Observation of the catalyst particles behavior during reduction *via* the selected-area microscopy allowed us to detect a level of changes in catalyst morphology.

A SiO_2 modified 90% Ni catalyst prepared by heterophase sol–gel technique was selected as a sample for the study. The procedure of the catalyst preparation has been described earlier.[19] The catalyst was previously studied by X-ray diffraction. The main component before reduction was Ni^{II} hydroxide, and Ni^{II} oxide was also present.

The study of morphology was carried out by scanning electron microscopy at three levels dependent on the size of the studied objects: macroscopic level — an ensemble of catalyst particles; microscopic level — individual catalyst particles and nanoscale level — the structure of individual catalyst particles and their subunits. An important aspect was to explore the selected identical location and the identical particles before and after the reduction procedure. The method of selected-area microscopy plays an important role in this work, inasmuch as considering different particles before and after reduction one can detect only a change in the average parameters of the sample. Whereas in this case, the morphology can vary without changing the average parameters.

For this purpose, a 10 mg sample was deposited on an aluminum microscopy stub. This amount of sample is appropriate for conducting studies of the catalytic activity. The particles were deposited on the stub in a single layer to ensure uniform heating and hydrogen availability.

Special attention in our experiment has been paid to the preservation of the particles adhesion to the stub at high hydrogenation temperatures (400 °C). This was achieved by using a carbon tape and a thin layer of glue to stick the catalyst particles directly to the aluminum table. Marks were placed on the sample stub to facilitate finding the selected group of particles. To confirm the general nature of the phenomenon, three groups of particles located at a distance of at least 5 mm from each other were selected. Moreover, to avoid the loss of selected particles during heating, three groups of particles have been investigated. During repeated microscopic examination after reduction, a recognizable area has been selected after recording each image to make it easier to find the right area containing selected group of particles and individual particles (Figure 1).

Before the reduction [Figure 1(*a*)], a region of the sample with 1 × 0.8 mm catalyst particles was examined at the macro level at ×100 magnification. Over 50 catalyst particles located in this area formed separate groups containing from 3 to 10 particles per group. The particle diameter ranged from 44 microns to 175 microns, the average diameter was 109.5 μm.

After the reduction [Figure 1(*b*)], the relative position of the particles varied, which resulted in the loss of some particles during reduction. The particles also formed separate groups with the mean count over 50 particles, while the average particle diameter remained unchanged — 109.5 μm.

A single catalyst particle at ×1000 magnification was selected to study the catalyst at the microlevel (Figure 2). The individual particles were irregular in shape and consisted of flakes. The flakes formed 3–4 pieces stacks of the average thickness of 31 nm.

After hydrogenation, it was possible to find the particle studied before the hydrogen treatment, which did not undergo changes in its location. At the scale of 50 μm, there were no visible changes on microscale level. Microscopy of the selected particle allowed us to show that the flakes did not change their relative position. The number of flakes in the stack and the distance between individual flakes also remained unchanged. At the same time, formation of new particles of average size 93 nm could be observed on the flakes. But these changes relate to nanoscale transformations. EDS mapping has shown uniform distribution of Ni and Si at the microlevel (Figures S41, S42).

At higher magnification, the catalyst was examined at the nanoscale level (Figure 3). Thus, at a ×100 000 magnification, it was seen that individual flakes have a smooth structure [Figure 3(*a*)]. After reduction at this magnification surface defects became clearly visible: bulges and depressions that modified the morphology of the flakes [Figure 3(*b*)]. It is obvious that the roughness of the flakes is caused by the formation of small individual nanoparticles (with average size of 13 nm) on the surface of the flakes [Figure 3(*c*)]. These defects can be explained by the alteration and deformation of the crystal lattice

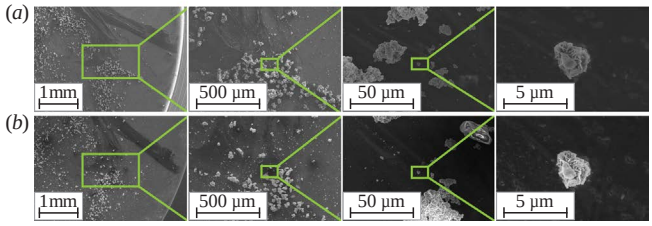

Figure 1 Particle tracking process using SEM: (*a*) before and (*b*) after reduction.

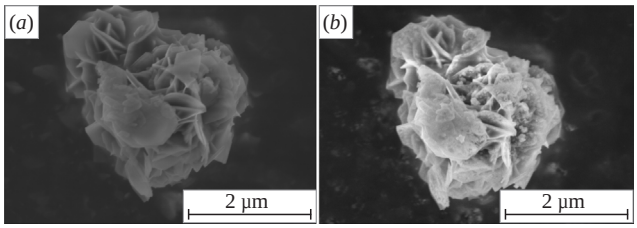

Figure 2 Comparison of the nickel catalyst particle (*a*) before and (*b*) after reduction.

on the crystallite surface due to the reduction of Ni^{II} to metallic nickel. According to TEM data, the average diameter of formed at 400 °C hydrogenation nanoparticles reached 66 nm (Figure S58) and average size of the nickel particles calculated from XRD data by Williamson–Hall method was 53 nm.

XRD data showed that the catalyst had undergone reduction under hydrogen treatment. In the XRD spectrum of the nickel catalyst before reduction, the main phase was Ni^{II} hydroxide and Ni^{II} oxide was also present. After reduction, the main phase was nickel metal. Only low-intensity Ni^{II} oxide signals were revealed. Thus, despite the absence of changes at the macro- and microlevels, the phase composition of the sample completely altered as a result of hydrogen reduction under 400 °C. This can indicate pseudomorphism of the observed reduced flakes.

It should be noted that no formation of such particles was observed under milder hydrogenation conditions (200 °C) (Figure S61) and in this case the XRD was identical to the original sample (Figure S60A). To exclude the effect of the support and sample preparation artifacts at selected area microscopy, an additional experiment was performed under harsher conditions (600 °C) without a stub for EM. Interestingly, the morphological change process goes further under these conditions, *i.e.*, flakes have been totally destroyed. And the average size of nanoparticles decreased: 16 nm according to XRD and 38 nm according to TEM (Figure S59). The results of the TEM and PDBSE showed a greater contrast of these particles against the background of the substance, which

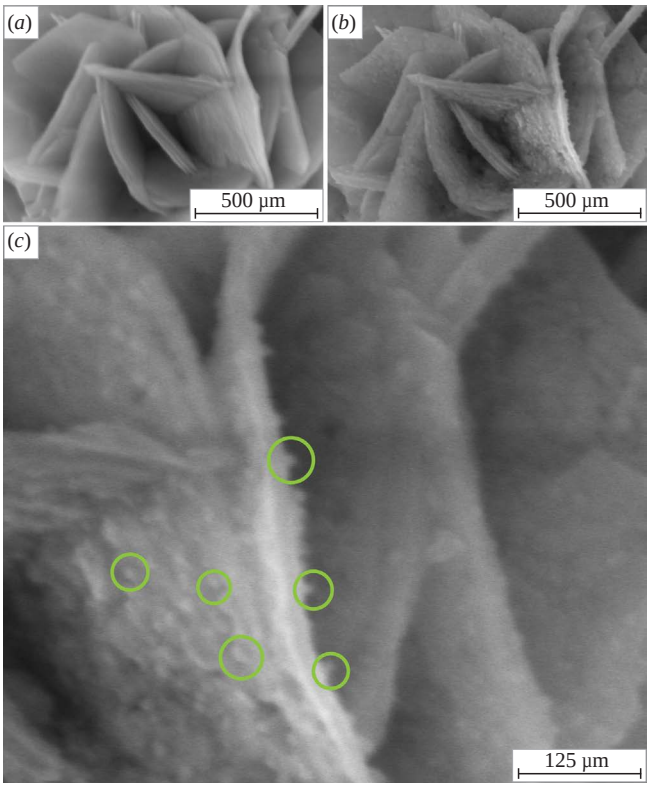

Figure 3 Comparison of the nickel catalyst particle (*a*) before and (*b*), (*c*) after reduction.

indicates their nickel nature (Figures S27–29, S34–36). The decrease in the average size of nanoparticles may be due to the fact that under harsher conditions nickel nanoparticles are formed from small parts of the destructed flakes at the last stage of hydrogenation. At the same time, the silicate shell can prevent sintering of the forming nickel nanoparticles and increase their average diameter.

SEM imaging of a selected group of a Ni^{II} hydroxide-based SiO_2 modified catalyst particles before and after hydrogen treatment allowed us to determine the effect of the catalyst reduction stage on modification the individual particles morphology. In the process of hydrogenation $Ni(OH)_2$ was converted to the active metal form. Changes were recorded at three levels: first, in the selected groups, the relative positions of particles did not change, except for the loss of particles due to support deformation and weak fixation; second, individual particles in all cases retained their size and shape and no changes in morphology were observed at the micro level; third, significant changes in the morphology of subunits (flakes) of catalyst particles were recorded at the nanoscale level. Deformation of the subunit surface and formation of nanostructures were observed. Based on the results of this study, it was found that noticeable changes in the morphology and size of the Ni catalyst were manifested at magnification of more than 10^5 times. Nanostructures of metallic nickel were formed.

Thus, hydrogen reduction of the catalyst not only promotes its activation by altering the phase composition but modifies catalyst operation in chemical reactions due to the formation of nanoscale structures. It is important to note that changes at the nanoscale level occur already under mild hydrogenation conditions at 400 °C. Destruction of flakes takes place under harsher conditions, but no increase of the average diameter of Ni nanoparticles has been observed. Thereby, the evolution of catalyst morphology can proceed without noticeable changes in the phase composition and average size of the catalyst particles. Herewith selection of the optimal hydrogenation conditions provides an additional tool for controlling the nanosized structure of the nickel catalyst.

Online Supplementary Materials

Supplementary data associated with this article can be found in the online version at doi: 10.1016/j.mencom.2024.10.041.

References

1 V. P. Ananikov, *ACS Catal.*, 2015, **5**, 1964; https://doi.org/10.1021/acscatal.5b00072.
2 A. L. Clevenger, R. M. Stolley, J. Aderibigbe and J. Louie, *Chem. Rev.*, 2020, **120**, 6124; https://doi.org/10.1021/acs.chemrev.9b00682.
3 A. Ghatak and M. Das, *ChemistrySelect*, 2021, **6**, 3656; https://doi.org/10.1002/slct.202100727.
4 Q.-Y. Guo, Z. Wang, X. Feng, Y. Fan and W. Lin, *Angew. Chem., Int. Ed.*, 2023, **62**, e202306905; https://doi.org/10.1002/anie.202306905.
5 M. R. Shamsuddin, N. Asikin-Mijan, T. S. Marliza, M. Miyamoto, S. Uemiya, M. A. Yarmo and Y. H. Taufiq-Yap, *RSC Adv.*, 2021, **11**, 6667; https://doi.org/10.1039/D0RA09246K.
6 R. Ye, L. Ma, X. Hong, T. R. Reina, W. Luo, L. Kang, G. Feng, R. Zhang, M. Fan, R. Zhang and J. Liu, *Angew. Chem., Int. Ed.*, 2024, **63**, e202317669; https://doi.org/10.1002/anie.202317669.
7 M. Stanković, J. Krstić, M. V. Gabrovska, V. Radonjić, D. Nikolova, D. Lončarević and D. Jovanović, in *New Advances in Hydrogenation Processes – Fundamentals and Applications*, 2017, pp. 131–179; https://doi.org/10.5772/66967.
8 J. Derosa, O. Apolinar, T. Kang, V. T. Tran and K. M. Engle, *Chem. Sci.*, 2020, **11**, 4287; https://doi.org/10.1039/C9SC06006E.
9 A. L. Kustov, T. R. Aymaletdinov, A. A. Shesterkina, K. B. Kalmykov, P. V. Pribytkov, I. V. Mishin, S. F. Dunaev and L. M. Kustov, *Mendeleev Commun.*, 2024, **34**, 221; https://doi.org/10.1016/j.mencom.2024.02.020.
10 A. V. Egorysheva, K. R. Plukchi, S. V. Golodukhina, E. Yu. Liberman and O. G. Ellert, *Mendeleev Commun.*, 2023, **33**, 608; https://doi.org/10.1016/j.mencom.2023.09.005.
11 Z. Fan, W. Weng, J. Zhou, D. Gu and W. Xiao, *J. Energy Chem.*, 2021, **58**, 415; https://doi.org/10.1016/j.jechem.2020.10.049.
12 A. R. Ardiyanti, M. V. Bykova, S. A. Khromova, W. Yin, R. H. Venderbosch, V. A. Yakovlev and H. J. Heeres, *Energy Fuels*, 2016, **30**, 1544; https://doi.org/10.1021/acs.energyfuels.5b02223.
13 Y. Shen and A. C. Lua, *J. Power Sources*, 2015, **280**, 467; https://doi.org/10.1016/j.jpowsour.2015.01.057.
14 Y. Shen and A. C. Lua, *RSC Adv.*, 2014, **4**, 42159; https://doi.org/10.1039/C4RA04379K.
15 M. Hadian, D. P. F. Marrevee, K. A. Buist, B. H. Reesink, A. N. R. Bos, A. P. Bavel van and J. A. M. Kuipers, *Chem. Eng. Sci.*, 2022, **260**, 117938; https://doi.org/10.1016/j.ces.2022.117938.
16 Y. K. Gulyaeva, M. V. Alekseeva (Bykova), D. Yu. Ermakov, O. A. Bulavchenko, O. O. Zaikina and V. A. Yakovlev, *Catalysts*, 2020, **10**, 1198; https://doi.org/10.3390/catal10101198.
17 P. Zhang, Y. Sun, M. Lu, J. Zhu, M. Li, Y. Shan, J. Shen and C. Song, *Energy Fuels*, 2019, **33**, 7696; https://doi.org/10.1021/acs.energyfuels.9b01538.
18 M. V. Chudakova, M. V. Popov, P. A. Korovchenko, E. O. Pentsak, A. R. Latypova, P. B. Kurmashov, A. A. Pimenov, E. A. Tsilimbaeva, I. S. Levin, A. G. Bannov and A. V. Kleymenov, *Chem. Eng. Sci.*, 2024, **284**, 119408; https://doi.org/10.1016/j.ces.2023.119408.
19 M. Popov, V. Maximov and V. Kogan, *MATEC Web of Conferences*, 2021, **340**, 01011; https://doi.org/10.1051/matecconf/202134001011.
20 O. S. Al-Ayed and D. Kunzru, *J. Appl. Chem. Biotechnol.*, 2007, **43**, 23; https://doi.org/10.1002/jctb.280430104.
21 D. Y. Ermakov, M. V. Bykova, S. A. Selisheva and S. A. Khromova, *Patent RU 2496580C1*, 2013.
22 V. A. Yakovlev, S. A. Khromova, D. Y. Ermakov, V. N. Parmon, R. H. Venderbosch, H. J. Heeres and A. R. Ardiyanti, *Patent RU 2440847C1*, 2012.
23 M. A. Ermakova and D. Yu. Ermakov, *Catal. Today*, 2002, **77**, 225; https://doi.org/10.1016/S0920-5861(02)00248-1.
24 M. A. Ermakova and D. Y. Ermakov, *Appl. Catal., A*, 2003, **245**, 277; https://doi.org/10.1016/S0926-860X(02)00648-8.
25 M. A. Ermakova, D. Yu. Ermakov, S. V. Cherepanova and L. M. Plyasova, *J. Phys. Chem. B*, 2002, **106**, 11922; https://doi.org/10.1021/jp021231q.
26 S. G. Zavarukhin and G. G. Kuvshinov, *Appl. Catal., A*, 2004, **272**, 219; https://doi.org/10.1016/j.apcata.2004.05.044.
27 W. Wang, H. Wang, Y. Yang and S. Jiang, *Int. J. Hydrogen Energy*, 2012, **37**, 9058; https://doi.org/10.1016/j.ijhydene.2012.03.003.
28 P. H. Blanco, C. Wu, J. A. Onwudili and P. T. Williams, *Appl. Catal., B*, 2013, **134**–**135**, 238; https://doi.org/10.1016/j.apcatb.2013.01.016.
29 J. Li, L. Zhao, J. He, L. Dong, L. Xiong, Y. Du, Y. Yang, H. Wang and S. Peng, *Fusion Eng. Des.*, 2016, **113**, 279; https://doi.org/10.1016/j.fusengdes.2016.06.046.
30 M. Afzal, C. R. Theocharis and S. Karim, *Colloid Polym. Sci.*, 1993, **271**, 1100; https://doi.org/10.1007/BF00659300.
31 D. B. Eremin and V. P. Ananikov, *Coord. Chem. Rev.*, 2017, **346**, 2; https://doi.org/10.1016/j.ccr.2016.12.021.
32 A. S. Galushko and V. P. Ananikov, *ACS Catal.*, 2024, **14**, 161; https://doi.org/10.1021/acscatal.3c03889.
33 E. D. Boyes, A. P. LaGrow, M. R. Ward, R. W. Mitchell and P. L. Gai, *Acc. Chem. Res.*, 2020, **53**, 390; https://doi.org/10.1021/acs.accounts.9b00500.
34 A. P. LaGrow, M. R. Ward, D. C. Lloyd, P. L. Gai and E. D. Boyes, *J. Am. Chem. Soc.*, 2017, **139**, 179; https://doi.org/10.1021/jacs.6b08842.
35 M. R. Ward, E. D. Boyes and P. L. Gai, *J. Phys.: Conf. Ser.*, 2014, **522**, 012068; https://doi.org/10.1088/1742-6596/522/1/012068.

Received: 22nd May 2024; Com. 24/7500